

DISCOVERY OF NEW FAINT RADIO EMISSION ON 8° TO 3' SCALES IN THE COMA FIELD,  
AND SOME GALACTIC AND EXTRAGALACTIC IMPLICATIONSP.P. KRONBERG<sup>1,2</sup>, R. KOTHES<sup>3,4</sup>, C.J. SALTER<sup>5</sup>, P. PERILLAT<sup>5</sup>*Draft version October 25, 2018*

## ABSTRACT

We present a deep, 8° diameter, 0.4 GHz radio image using a first time combination of the NAIC Arecibo 305-m telescope in Puerto Rico, and the wide-angle interferometer at the Dominion Radio Astrophysical Observatory at Penticton, Canada. Our observations are centered on the Coma Cluster of galaxies in the “Great Wall” of galaxies near the North Galactic Pole. The complementary nature of these two instruments enables us to produce a distortion-free image that is sensitive to radiation on scales from 8° down to that of an individual galaxy halo at the 100 Mpc distance of the Great Wall. Newly revealed patches of distributed radio “glow” are seen well above the detection limit. One prominent such area coincides with groupings of radio galaxies near the Coma cluster, and indicates intergalactic IGM magnetic fields in the range 0.2 to 0.4  $\mu$ G on scales of up to  $\sim 4$  Mpc. Other patches of diffuse emission, not previously explored at these high latitudes on arcminute scales, probably contain Galactic “cirrus”. A striking anticorrelation is found between low-level diffuse radio glow and some regions of enhanced optical galaxy surface density, suggesting that cosmological Large Scale Structure (LSS), normally defined by the baryonic (or dark) matter density, is not *uniquely* traced by faint continuum radio glow. Rather, intergalactic diffuse synchrotron radiation represents IGM magnetic and Cosmic ray energy density, instead of matter density. The diffuse, arcminute-level structures over a large region of sky are potentially important pathfinders to CMB foreground radiation on high multipole scales.

## 1. INTRODUCTION

The existence of magnetic fields in and near the periphery of clusters of galaxies, and their implied  $\mu$ G-level strengths, leads naturally to the question as to whether significant fields exist on yet larger scales in the intergalactic medium (IGM), namely on the scale of galaxy filaments in cosmological large scale structure (LSS). If so, important objectives are (1) to investigate the intergalactic magnetic field strength and structure, (2) to determine the excitation state and metallicity of any associated warm-hot intergalactic medium (WHIM) (e.g. Henry 2004, Nicastro et al. 2005), (3) to understand the intergalactic Cosmic Ray spectrum (e.g. Colgate & Li, 2004), and (4) to define the propagation environment of Ultra High Energy Cosmic Rays (UHECR’s) (e.g. Sigl et al. 2004). The achievement of these goals is ultimately important for solving important puzzles in high energy astrophysics, astro-particle physics, the origin of cosmic magnetic fields, and the evolution of LSS. Evidence for diffuse low frequency ( $\lesssim 30$  MHz) radiation in the Coma cluster vicinity at low resolution and low dynamic range has been presented in earlier work (e.g. Roger, Bridle, & Costain, 1973, Henning 1989). More sensitive and accurate arcminute resolution images (e.g. Kim et al. 1989 (0.3 GHz), Enßlin et al 1999 (74 MHz) have clarified the distribution of diffuse radiation, hence intergalactic magnetic field strengths in the near environs of the Coma cluster. The first attempt to probe magnetic field strengths on larger local-universe scales via Faraday rotation is described by Xu et al. (2006).

Both the feedback of outflows driven by galactic black holes (BH) (e.g. Furlanetto & Loeb 2001, Kronberg et al. 2001, Gopal-Krishna & Wiita 2001) and the gravitationally-driven evolution of large scale cosmic filament structure (e.g. Ryu, Kang & Biermann 1998, Dolag et al 2004) affect the physics of the IGM. Therefore, to understand both galaxy and LSS evolution over the redshift range of  $0 < z \lesssim 15$ , it is important to determine the strength and structure of intergalactic magnetic fields on size scales  $\sim 3 - 100$  times that of galaxy clusters.

Faint synchrotron radiation is a sensitive indicator of widespread magnetic fields. The detection of weak radio emission from cosmic ray electrons gyrating in intergalactic magnetic fields requires high sensitivity to *both* large and small scale structures at frequencies low enough that the spectral density of the synchrotron radiation is relatively high. While most radio interferometers can provide sensitive images of small scale structure, they inherently filter out structures broader than the angular size corresponding to their shortest spacings. In contrast, the largest single-dish antennas, with low noise receivers and vast collecting areas, provide enhanced surface brightness sensitivity for the detection of faint large scale emission. However, these have insufficient resolution to resolve blends of discrete radio sources. Motivated by the topical questions (1) - (4) above, we have combined the sensitivity of a very large single reflector with a well calibrated, wide-field interferometer to obtain a sensitive and precise image over a range of angular scales from 3' to those that

<sup>1</sup>IGPP, Los Alamos National Laboratory, Los Alamos NM USA<sup>2</sup>Department of Physics, University of Toronto, 60 St. George Street, Toronto M5S 1A7, Canada<sup>3</sup>National Research Council of Canada, Herzberg Institute of Astrophysics, Dominion Radio Astrophysical Observatory P.O. Box 248, Penticton, British Columbia, V2A 6K3, Canada<sup>4</sup>Department of Physics and Astronomy, University of Calgary, 2500 University Drive N.W., Calgary, AB, Canada<sup>5</sup>Arecibo Observatory, HC3 Box 53995, Arecibo, PR 00612, USA

overlap degree-scale all-sky surveys.

## 2. THE OBSERVATIONAL APPROACH

To overcome the spatial frequency coverage problems mentioned in §1, we have used the unprecedented combination of the 305-m Arecibo radio telescope and the wide-field interferometer telescope of the Dominion Radio Astrophysical Observatory (DRAO) at Penticton, observing at frequencies near 0.4 GHz. The resultant resolution is comparable to that of a 1000-m single-dish telescope. Fortunately, the area near the North Galactic Pole that we have imaged lies within the limited declination range accessible to both telescopes. DRAO interferometer data were also collected in spectral line mode near 1.4 GHz, though these are not discussed here. The DRAO interferometer has 9-m diameter dishes and a maximum baseline length of 617 m. This combination of the largest single antenna with the precision imaging capabilities of the DRAO interferometer can produce distortion-free images at 0.4 GHz on all angular scales from 3' to 8°. The combination gives a large overlap in spatial frequency, enabling an effective cross-calibration of the Arecibo and DRAO data in  $u$ - $v$  space to optimize image reliability.

We chose to observe a section of the Great Wall centered on the Coma cluster of galaxies (at  $z=0.02320$ , or  $100h_{70}^{-1}$  Mpc distance). The linear resolution at 100 Mpc is  $\sim 120$  kpc at full resolution, close to a galaxy halo scale at the Great Wall, and hence favorable for separating individual radio sources from true diffuse radiation.

The DRAO interferometer, having only East-West spacings, has no geometrical “ $w$ ” component. Consequently, in a single pointing at 408 MHz it produces a distortion-free image over the entire  $9.5^\circ$  (to the 10% response level) of the primary beam, whose FWHM is  $5.5^\circ$ . This, along with the large spatial frequency overlap, makes it straightforward in principle to combine the DRAO data with the raster-scanned Arecibo images to undertake sensitive, high-precision, wide-area radiometry in a single pointing. The result is a combination of image fidelity and surface brightness sensitivity that is unprecedented for this frequency and resolution range over a large field of sky.

## 3. OBSERVATIONS AND DATA PROCESSING

### 3.1. Observations with DRAO

The DRAO antenna feeds are mounted at the prime focus and simultaneously accept radiation at 1420 MHz in both circular polarizations, and at 408 MHz in right-hand polarization only. At the center of our maps the synthesized beam has dimensions of  $2.8 \times 6.7$  (R.A.  $\times$  Dec.) at 408 MHz. A detailed description of the DRAO Synthesis Telescope can be found in Landecker et al. (2000).

With the DRAO Synthesis Telescope, we observed two pointings towards the Coma Cluster. These were centered at:  $\alpha(\text{J2000}) = 12^h 57^m 55^s$ ,  $\delta(\text{J2000}) = +27^\circ 39'$  and  $\alpha(\text{J2000}) = 12^h 57^m 55^s$ ,  $\delta(\text{J2000}) = +28^\circ 09'$ , i.e. the two field centers differed by  $30'$  in Declination. This served as an additional check against artifacts in low-level diffuse structure, and provided a  $\sqrt{2}$  improvement in overall signal to noise.

A full synthesis at each pointing consisted of 12 individual 12 hr observations. Each 12 hr run had a different configuration of the three (of seven) movable antennas

along a precision railway track. Thus, the measurements for the two pointings extended over a total of 24 12-hour days, and took place in Spring 2003. Complex gains for the pointing centers were calibrated by observing the unresolved sources 3C147 and 3C295. Their flux densities at 408 MHz are 48 Jy and 54 Jy, respectively. The rms noise level on the image from the combined DRAO pointings was  $\sim 2.9$  mJy/beam, which corresponds to  $\sim 300$  mK.

Phase and amplitude drifts over each 12 hr observing interval were corrected via self-calibration. At this point, many strong compact sources have remaining ring artifacts, and these are removed by a procedure called MODCAL, which uses the CLEAN source components as its input model. The image processing routines were developed specifically for the DRAO Synthesis Telescope and are described in Willis (1999). Due to an interferometer’s lack of zero spacing information, negative bowls appear around extended sources. Residual rings around compact sources located in these bowls are hidden because the peak of the source is lower than its true value, and may even be at a negative level. To overcome this problem, extended and fine scale structure were CLEANed separately at the end of the data processing. Amplitude self calibration can produce slight flux density scale errors in the individual observations. For this reason we used the original unprocessed but properly calibrated image to re-calibrate the final DRAO image using all point sources with flux densities above  $10 \sigma$ . The required corrections for each of the two final images were less than 5%.

### 3.2. Observations with Arecibo

The 305-m Arecibo telescope has been upgraded by the addition of a 25-m dome containing secondary and tertiary reflectors. These illuminate an effective surface area of about 225-m diameter. The overall rms surface accuracy, including the primary surface upgrade is  $\sim 2$  mm, and the beam size is  $10' \times 12'$  at 430 MHz. The Arecibo observations were taken during multi-night sessions in the springs of 2003 and 2004. The system temperature was  $\sim 55$  K, of which  $\sim 20$  K comes from the sky at the NGP. The receiver bandwidth was 20 MHz at a center frequency of 430 MHz. We recorded right- and left-hand circular polarization channels for each of four overlapping sub-fields. Each sub-field was covered by two orthogonal (R.A./Dec.) sets of raster scans recorded in spectral line mode. After the removal of interfered frequency channels in both time and frequency domains, and calibration, the orthogonal coverages were optimized using the basket-weaving technique (Sieber et al. 1979). Using reduction techniques that were custom developed at Arecibo, the orthogonally scanned sub-fields were then merged to form a single  $8^\circ$  by  $8^\circ$  image whose center coincided with that of the combined pair of DRAO fields. The Arecibo beam pattern was measured separately on the radio bright galaxy 3C433, so that the final Arecibo image could be beam-deconvolved. Zenith Angle-Azimuth variations of  $T_{sys}$  at 430 MHz are well determined, and were calibrated out. The basketweaving and field combination techniques were effective to the point where any residual striations from raster scanning were so faint that they were a small fraction of the final noise level and could no longer be seen visually in the images. The theoretical thermal noise level of our Arecibo image is 4.2

mK. For absolute temperature calibration we used the the 408-MHz all-sky map of Haslam et al.(1982) with an adjustment, described below, for the small difference in sky frequencies.

### 3.3. Combination of the Data Sets

The lower spatial frequency limit of an interferometer observation is determined by the shortest antenna spacing present. For the DRAO synthesis telescope this is about 13 m, which translates to about  $3^\circ$  on the sky at 408 MHz. To achieve complete spatial frequency coverage, the missing information on larger structures must be obtained from our Arecibo 430-MHz observations, and for absolute radiometric calibration we again used the 408-MHz all-sky map of Haslam et al. (1982). Since the Arecibo map was at 430 MHz, we had to extrapolate these data to the DRAO center frequency of 408 MHz. This procedure was based on an inter-comparison of the flux densities of compact sources above 1 Jy in the DRAO and Arecibo maps. An average flux density ( $S$ ) scaling factor of  $1.05 \pm 0.03$  was determined, corresponding to a spectral index of  $\alpha = -0.9$ , defined by  $S \propto \nu^\alpha$ . The lowest and highest individual ratios were 0.98 and 1.12. This is a reasonable result for compact extragalactic radio sources. After the appropriate scaling, the Arecibo map was combined with the two individual DRAO pointings separately, after suitable filtering in the Fourier domain and applying the DRAO primary beam correction.

Before merging the single-dish and interferometer data, the Arecibo image was converted into visibilities by Fourier-transforming, and removing the Arecibo beam by dividing by the transform of the beam pattern. The resulting image was multiplied by the DRAO primary beam to create a short spacing map that complements the interferometer data. Then the two data sets were merged in the  $u$ - $v$  plane using a normalized tapering function in the overlap area. At this point the two resulting maps were primary beam corrected and then co-averaged.

To confirm the flux density scaling, we used all compact sources above 200 mJy in the inner area of our final map. The flux densities were compared with those published in Kim (1994). A linear fit gives a gradient of  $1.00 \pm 0.02$  (see Fig. 1). The actual r.m.s. noise in the final image at full resolution is about 360 mK, which translates to 3.2 mJy/beam. This includes “confusion” due to weak background sources, residual scanning noise at Arecibo, residual fluctuations in the Arecibo  $T_{sys}$  calibration, an unknown Galactic disc plus halo contribution, and any diffuse extragalactic emission.

## 4. THE IMAGES

Fig. 2 shows a combined Arecibo + DRAO + Effelsberg image at the full DRAO resolution of  $2.8' \times 6.7'$ . It excludes the outermost zone of the DRAO primary beam beyond an  $8^\circ$  diameter circle. This image clearly shows patches of diffuse radiation. The patterns of diffuse emission are particularly apparent after the subtraction of discrete sources. This is seen in Fig. 3 which, like Fig. 2, is at the full resolution and has complete  $u$ - $v$  coverage. Figs. 4 and 5 present the image with the discrete sources subtracted (as in Fig. 3) and smoothed to a resolution of  $10' \times 10'$ , close to the FWHM of the Arecibo telescope. The images are discussed below.

### 4.1. Checks on image reliability

To further investigate the reliability and nature of the diffuse patches, we have compared the independent DRAO pointings, and examined the effects of removing the point sources. This tests whether some of the diffuse patches could be a residual summation of incompletely removed sidelobes of the many discrete sources. We found that discrete radio sources have no detectable effect on the level and distribution of the diffuse structure.

Another image, not shown, was made using only the DRAO data (i.e. without Effelsberg or Arecibo), and convolved to the  $10'$  resolution of the Arecibo telescope. Virtually all of the larger scale features in Figs. 4 and 5 could be recognized, although with poorer definition and signal to noise. Also, significantly, when the Arecibo data were added with the optimal ( $u,v$ ) overlap range (see below) no new strong large scale features were introduced.

The possibility of Solar interference in the far-out sidelobes of the DRAO array was also investigated. The Sun was above the horizon for less than 20% of the two DRAO observing runs. While risen, its Hour Angle relative to the Coma field,  $\Delta(\text{HA})$ , was large, and varied over the 2-month period of the DRAO observations. No systematic Solar-related effects were identified.

Another conceivable cause of image artifacts could, in principle, arise at the shortest spacings of the small DRAO dishes where direct feed-to-feed electromagnetic interaction could occur. To test for this effect, we re-imaged the DRAO data removing the shortest physical separations in two steps ( $< 25$  m and  $< 50$  m). The images were unaffected, except for the expected small effects at the largest image scales from removing genuine, low ( $u,v$ ) components. We also subtracted these images from the final maps (which removes all small-scale structure) and inspected these for low-level “striping” that might have artificially produced diffuse patches. We found no evidence of a spurious origin for any of the diffuse features due to short-spacing interactions.

An important test of the Arecibo-DRAO combined image reliability is to examine the effect of varying the upper and lower limits of the overlap zone in ( $u,v$ ) space between the two instruments. This is important to investigate, since the 0.4 GHz Arecibo telescope beam, although very stable at a given pointing, has systematic beam squint and beam pattern variations over the range of [AZ-ZA] pointing directions. Since our measured Arecibo beam averages out such variations, a beam deconvolution will introduce systematic errors at the larger  $|u,v|$  values in the Fourier-transformed Arecibo image. By varying the  $|u,v|$  overlap zones between the 305-m and DRAO telescopes we were able to find an optimal maximum  $u$ - $v$  limit for the Arecibo data below which no distortions are introduced in the combined image. An additional, and largely independent, criterion is to test for consistency with the smoothed “DRAO-only” image described above. Our final Arecibo “[ $u,v$ ] low-pass” filter limit was set at 75 m. This limit leaves considerable Arecibo-DRAO overlap, and retains the Arecibo sensitivity to the most important large scales in respect of diffuse emission.

### 4.2. Nature and location of the diffuse patches

In Figs. 3-5 we show the combined, full-resolution image from which we have subtracted (CLEANed) the discrete sources, except for the diffuse halo of the Coma cluster itself.

Several patches of diffuse emission can be seen both at the higher 3' DRAO resolution in Figs. 1 and 2, and at the  $\sim 10'$  resolution of the Arecibo Telescope. In the absence of additional information these could be either galactic or extragalactic in origin. They are seen for the first time at these faint levels and small scales at high Galactic latitude. Many of them probably represent Galactic foreground emission, while others might be regions of extragalactic emission at the Great Wall, or beyond. In this section we discuss the features in some detail, in particular the two particularly bright features, which are labelled A and B in Fig. 5.

At the outer periphery of our images, the DRAO interferometer's image noise level deteriorates by a factor of  $\sim 2$  and the discrete source subtraction there might lack the precision it has over the rest of the field. Thus, extended features close to the image periphery could contain some imaging systematics.

The most prominent diffuse feature (A) near the Coma cluster's halo has a clear morphological connection with the Coma cluster halo. This connection is seen at both resolutions, and is especially evident in figs 2, 4, and 5.

The inner, brighter parts of this diffuse region immediately west of the Coma cluster have been independently detected at 326 MHz by Kim et al. (1989), at 1.4 GHz by Deiss et al. (1997), and at 74 MHz by Enßlin et al. (1999). It also overlaps the diffuse, "satellite" X-ray source in the 0.5 - 2.4 keV band (White, Briel and Henry, 1993). We explain in section 4.5 why the X-ray surface brightness distribution is unlikely to correlate 1:1 with the radio emission of Region A.

Region A appears as a complex of enhanced radio emission that extends to a maximum of  $\sim 2.1^\circ$  ( $3.7 h_{70}^{-1}$  Mpc) west of the center of the Coma cluster's radio halo as defined by the 2.25K contour in Figure 4. Our most conservative estimate of this limit is  $\approx 1.4^\circ$  ( $2.4 h_{70}^{-1}$  Mpc). At  $10'$  resolution its surface brightness is consistently  $> 2.25\text{K}$  over a large area (Fig. 4), in contrast to other surrounding emission. Region A is also partly superimposed on a "landscape" of other diffuse radiation at brightness levels from  $\lesssim 1.4\text{K}$  to  $\sim 2\text{K} \approx 7\sigma$  (Figure 5). These are the extended regions to the north and south of A, and to the southeast of the Coma cluster itself. The 2.25K contour in Figure 4 was chosen to illustrate that region A contains a broad component of emission that is consistently elevated above this background, even though its detailed  $T_B$  variations will be modulated by the underlying  $\Delta T$  fluctuations just mentioned which are  $\lesssim 1\text{K}$ . Besides this broad component region A also contains complex stronger substructures having  $T_B$  up to  $3\text{K}$  ( $15\sigma$  above baseline confusion) and above. This can be seen in Fig. 5, and also the brightest parts of the images in Figs 2 and 3 (both at  $2.8' \times 6.7'$  resolution). Both these brighter and patchier areas and the broader emission show a clear contiguity with the Coma cluster's radio halo. Independently, region A also coincides approximately with an unusual grouping of 7 radio galaxies, *all* at redshifts near the Great Wall, and which lie approximately within the boundaries of re-

gion A (Refer to Figs 2 and 5). For all of the above reasons we conclude that region A and certainly its brighter components are most likely extragalactic, and associated with the Great Wall. The uncertainty in region A's outer boundaries is due to possible superimposition with other large scale features mentioned above, which are possibly of Galactic origin.

A second diffuse feature, B, is clearly seen on each DRAO image. Its extent and total flux density are even better defined when combined with the Arecibo data. Feature B is the relatively bright diffuse patch near  $\alpha = 12^h 59^m$ ,  $\delta = +30.3^\circ$ , centered about  $2.5^\circ$  directly north of the Coma Cluster. It is best seen in Figs. 4 and 5. Its dimensions ( $\lesssim 1^\circ$ ), and relatively high surface brightness suggest that it too is extragalactic, possibly a giant, relic radio galaxy. Its integrated flux density at 0.4 GHz is  $\sim 1.5$  Jy, and its peak surface brightness is  $\sim 4$  K. It is illustrative to compare this surface brightness with the rms sensitivity,  $\Delta T_{rms} \sim 0.14$  K, of the 1.4 GHz NVSS survey (Condon et al. 1998), currently a widely used and benchmark radio source catalog. At 1.4 GHz, the peak  $T_B$  of feature B, scaled with  $\alpha = -1$  to 1.4 GHz would be  $100$  mK, or  $0.33$  mJy/beam in the NVSS survey. This is a factor of  $\sim 7$  below the faintest reliably detected source in the NVSS survey ( $2.3$  mJy at 1.4 GHz), and just below  $\Delta T_{rms}$  of the NVSS.

At the higher resolution of Figs. 2 and 3, the northern end of feature B appears to contain a "cluster" of faint discrete sources. The peak 0.4 GHz flux densities of these unresolved sources are  $\lesssim 3$  mJy/beam at our  $2'8 \times 6'7$  resolution. Returning to our check for detectability in the NVSS, their corresponding 1.4 GHz flux densities would be  $\lesssim 1$  mJy/beam (for  $\alpha \sim -1$ ), which is also below the NVSS detection limit.

The comparisons above illustrate how even some of the brightest diffuse emission features can escape detection in discrete radio source catalogs. It further demonstrates the advantage of full  $u-v$  coverage with high sensitivity at the lowest  $uv$  spacings. Source B has no obvious optical identification, which is not surprising in view of its large angular size. It seems most likely that it is near the Great Wall, or even beyond. We think it unlikely to be Galactic, on the basis of its relatively high surface brightness this close to the NGP, and the small cluster of faint discrete sources that appear projected against it (Fig. 2). However, at this stage we cannot entirely rule out some Galactic contribution.

Many other apparently diffuse features appear unrelated to regions A and B. They could be Galactic foregrounds seen for the first time at this sensitivity and resolution, and/or combinations of extragalactic diffuse emission and aggregates of faint, unresolved discrete sources.

#### 4.3. Comparison with nearby galaxy distributions

Fig. 4 shows the combined DRAO-Arecibo image after removal of the discrete sources and convolved to a  $10' \times 10'$  beam. Here, and in Fig. 5 we have also removed a  $22\text{K} - 16\text{K}$  linear plane approximation to the very broad emission structure derived from the Haslam et al. (1982) 408-MHz survey.

To compare the diffuse patches with optically visible galaxies, we show an overlay of galaxies in the CfA2 cat-

alog, color coded by radial velocity slice between 4,000 and 10,000 km/s (Huchra et al. 1990, de Lapparent et al. 1991). The radio glow in region A coincides with a galaxy overdensity zone to the west of the Coma Cluster, although the correspondence is not exact. This lack of detailed correspondence between diffuse radio emission and Great Wall galaxies appears to be general within this field. This statement can be further tested with a search for other galaxy clusters. Our field is large enough to include two additional clusters, having  $v = 38,000$  and  $70,000$  km/s, respectively, in an extension of the CfA survey (Huchra et al. 2004). These are approximately superimposed, lying within  $03^h 06^m < \alpha < 03^h 10^m$ ,  $29^\circ < \delta < 30^\circ$  (inset in Fig. 4). We find this region of high galaxy column density to have no detectable diffuse radio emission above  $\sim 200$  mK. This shows that dense groupings of galaxies are not *uniquely* associated with regions of radio glow, although clearly this does happen in some galaxy clusters and groups that have anomalously strong radio halos, such as the Coma cluster.

#### 4.4. Comparison of low-level glow with discrete radio source locations

Fig. 5 shows the same radio emission as Fig. 4, again at  $10'$  resolution, on which we have superimposed the strongest discrete radio sources from Fig. 2. Some groupings of discrete radio sources appear to correspond with areas of radio glow, and especially with region A. We recall that radio glow due to image spillover from these discrete sources has been ruled out.

Conversely, the intensity minima of our image, discussed below, show a tendency to not contain strong discrete radio sources. This apparent trend is interesting, but needs statistical confirmation from additional, similarly imaged, fields. This we are now undertaking. Discrete extragalactic radio sources are galaxies containing AGNs which, over a Hubble time, are expected to “feed back” energy into the IGM in the form of ejected cosmic rays (CRs) and magnetic fields. Global values for the intergalactic magnetic field strengths in galaxy filaments of LSS due to AGN feedback have been estimated to be of order  $10^{-7}$  G (Kronberg et al. 2001), and the global energy released in magnetized CR electron plasma is comparable to that released via quasar photons (e.g. Choksi and Turner, 1992). Generally, the discrete radio sources appear to be projected against the zones of radio glow. This trend, most apparent in Region A – see below, suggests that we may for the first time be seeing direct evidence in support of the BH–IGM feedback scenario in which the gravitational infall energy of central BH’s is injected into the surrounding IGM via radio jets and lobes. If so, over time the CR electrons in these zones will eventually cease to be visible at cm wavelengths, but will retain much of their magnetic energy, and possibly their CR proton energy, over much of a Hubble time.

#### 4.5. Physical characteristics of region A

In this section, for the reasons discussed in section 4.2, we proceed on the assumption that region A is a truly extragalactic complex at the approximate distance of the Great Wall, and not a foreground Galactic feature. Because it is also superimposed on other, we presume un-

related, extended features its outer boundaries cannot be precisely delineated, but this level of uncertainty does not significantly affect our discussion which follows.

The observed 0.4 GHz surface brightness leads to approximate estimates of intergalactic magnetic field strengths and total energy in region A assuming equipartition of energy between relativistic particles and magnetic fields. Adopting a parameter-space range that allows for different underlying background contributions to  $T_B$  in region A (giving total 408 MHz flux density extremes of  $\sim 0.8$  and  $3$  Jy), a volume filling factor of 0.1 and relativistic proton/electron energy ratios ( $k$ ) ranging from 1 to 100, we derive magnetic field strengths in the range of 0.2 to 0.4  $\mu$ G in this intergalactic region. The corresponding total energy is  $\sim 10^{59}$  to  $10^{60}$  ergs.

The radiating electrons do not appear to come from a single radio galaxy, and it is likely that the radio glow in region A comes at least partly from the aggregate activity, present and past, of radio galaxies near the redshift of the Coma cluster. To illustrate this, we identify a selection of co-located radio galaxies in Fig. 5, with their radial velocities listed in the figure caption. These are taken from the radio-optical identification list in Table 8 of Kim et al. (1994), to which we have added 3C277.3, (No. 8, at the unrelated  $v = 25583$  km s $^{-1}$ ), as a convenient reference source.

An additional energization could come from heating caused by gravitational infall as suggested by the distributed X-ray emission in this general area. An analysis of ROSAT all-sky survey PSPC data around Coma (Briel et al. 1992) shows diffuse X-ray emission covering part of region A. In projection, the diffuse X-ray emission contours presented by Briel et al. “fill” part, but not all, of the radio glow region A. A visual intercomparison of our Fig. 5 with Fig. 1 of Briel et al. is facilitated for the reader by the common location of source No. 9 (NGC4789) in Fig. 5 with its location in the X-ray image. It lies at the limit of region A and well beyond the outer X-ray contour of the diffuse “Coma-companion” X-ray source. However, Briel et al. report that ROSAT PSPC data reveal further, faint, and presumably unquantifiable, X-ray glow out to about  $1.6^\circ$  from the cluster center. This finding has been confirmed by Finoguenov et al. (2003) from XMM data.

The diffuse X-ray emission west of Coma appears to be mostly thermal (Briel et al. 1992, Finoguenov et al. 2003). However, the CR electron energy losses from region A will occur mostly by inverse Compton (IC) scattering of CMB photons, as we demonstrate below. This raises the question as to whether some (perhaps small) fraction of the X-ray luminosity seen by Briel et al. (1992) could be IC emission from region A. The electron energies ( $\gamma_e = E_e/mc^2$ ) in equipartition with a 0.3  $\mu$ G magnetic field range from  $\gamma_e \sim 10^4$  to  $10^5$ , so that the up-scattered CMB photons are broadly in the range of 0.3 MeV. This would make them virtually undetectable at the  $< 10$  keV energies where the ROSAT, Chandra and XMM satellites are most sensitive, though some keV-level photons could be produced if  $\gamma_e \lesssim 10^3$ . This is consistent with the finding that at least most of the 0.5 - 2 keV X-rays in this region are mostly thermal in origin, and not more than a modest fraction can come from the CR electrons that we detect in region A. It suggests that future radio–X-ray

comparisons to higher energy X- and  $\gamma$ -ray bands will reveal much more about the physics of this interesting and relatively energetic IGM zone. It also confirms, as we find and would expect, that the thermal Coma satellite X-ray emission does not mirror the details of the radio brightness structure of region A.

The requisite instrumental sensitivity in these higher energy photon bands is unfortunately not yet available. In future, very precise determinations of the thermal fraction of 0.5 - 2 keV X-rays from region A could in principle be used to test equipartition, by limiting the low- $\gamma$  end of the CR electron spectrum.

The energization associated with the thermal X-ray emission is thought to come from the infall of at least two subgroups toward the Coma cluster. These are associated with NGC 4839 and 4911 (Colless and Dunn, 1996). Another large scale gravitational energy source could be from infalling WHIM gas of neighboring cosmic filaments. The latter are broadly consistent with the simulations of Miniati et al. (2000), and are also concordant with the hot X-ray gas seen around the Coma cluster by Finoguenov et al. (2003). All of this suggests that the CR heating of the synchrotron-emitting electrons in Region A may have two sources; (1) that from AGN driven outflow discussed above that is ultimately provided by gravitational infall energy into the galaxy nuclei, and (2) from large scale gravitational infall that is implied from the velocity fields and perhaps the hot X-ray emitting gas.

It is interesting to compare estimated CR diffusion times with the electron energy loss times (synchrotron and IC) at 0.4 GHz. If the CR's have diffused from a multiplicity of AGN in the area as speculated above, the CR diffusion times,  $\tau_D$ , for an average distance to the nearest AGN inside the  $\sim 2$  - 3.8 Mpc dimensions of region A is the typical transport distance,  $L$  divided by the diffusion speed  $V_D$ . Normalizing to  $V_D = 1000$  km/s, comparable to an IGM sound speed, and  $L \sim 1.8$  Mpc,  $\approx$  half the size of region A, we get

$$\tau_D \approx 1.7 \times 10^9 \left( \frac{L}{1.8 \text{ Mpc}} \right) \left( \frac{1000 \text{ km/s}}{V_D} \right) \text{ yr} \quad (1)$$

This can be compared with the electron radiative loss times,  $\tau_R$ , which in this system are dominated by IC scattering against CMB photons:

$$\tau_R \approx \frac{2.8 \times 10^8 B_{0.3\mu\text{G}}^{1/2}}{\{B_{cmb}^2(1+z)^4 + (0.3B_{0.3\mu\text{G}})^2\} \left\{ \frac{v(1+z)}{0.4\text{GHz}} \right\}^{1/2}} \text{ yr} \quad (2)$$

where  $B_{cmb} \simeq 3.3 \mu\text{G}$  is the magnetic field that is equivalent in energy density to the CMB radiation. For the parameters adopted above,  $\tau_R$  is roughly an order of magnitude less than  $\tau_D$ . Unless relativistic particle diffusion times from their host galaxies are far above 1000 km/s, i.e., well above the IGM sound and magnetosonic speeds, this suggests that *in situ* acceleration of CR electrons exist in the rarefied magnetoplasma of intergalactic space *outside* of individual radio source lobes and galaxy clusters. Evidence for distributed particle acceleration has previously been deduced within the largest giant radio galaxies (e.g. Kronberg et al. 2004) which can have comparable dimensions to region A. In some cases, these have been imaged

near 10 GHz, where  $\tau_R$  is significantly smaller. At our imaging frequency of 0.4 GHz, this apparent contradiction could be removed if, for example,  $V_D$ , poorly known at this stage, were 10,000 km/s (3% of  $c$ ).

This comparison illustrates the importance of extending comparable observations to  $\gtrsim 10$  GHz using a next-generation radio telescope such as the proposed ‘‘Square Kilometer Array (SKA)’’, and at larger redshifts where radiative (IC) lifetimes are significantly shorter. Assuming the extragalactic dimensions of Region A, our observations place interesting constraints on the combination of  $V_D$  and  $\tau_R$ . Future, similar observations at higher frequencies, can provide tighter constraints on  $V_D$  for an intergalactic CR magnetoplasma, since  $B_{cmb}^2$  is known exactly, and  $B_{equipartition}$  can be reasonably well determined. This may constitute one of the few possibilities for *experimentally* estimating CR diffusion/transport speeds in extragalactic space.

#### 4.6. Comparisons with CMB fluctuations at $\approx 30$ GHz

It is of interest to extrapolate the surface brightness fluctuations in Figs. 3 & 5 to 30 GHz, at which frequency CMB fluctuations are imaged with similar angular scales. Assuming a constant radio spectral index of  $\alpha = -1$ , fluctuations of our diffuse radiation at 0.4 GHz, whether Galactic or extragalactic in origin, translate to  $\Delta T \approx 6.2 \cdot 10^{-6}$  K, at 32 GHz, or  $\Delta T/T_{cmb} \approx 2.3 \cdot 10^{-6}$ . If most of the  $\Delta T$  fluctuations in our images are extragalactic, we would not expect to see background synchrotron radiation fluctuations at  $\approx 30$  GHz on these scales unless there is some space-filling re-acceleration mechanism on supagalactic scales. This adds further interest to the question of IGM *in situ* acceleration raised in the previous section. Alternatively, if some of the arcminute-scale fluctuations are Galactic foreground, there is a greater possibility that a CMB foreground  $\Delta T/T$  effect could persist into the GHz range. Alternatively stated, to how high in frequency can the fluctuations seen in our maps be detected? This question again stresses the importance of future maps at frequencies  $\gg 1$  GHz to complement the capabilities of future low frequency telescopes operating below  $\sim 100$  MHz. It also highlights the importance of searching for, and identifying, foregrounds to CMB fluctuations. To achieve this, one would compare images such as those here near 400 MHz with others at successively higher frequencies in the 1 - 30 GHz range. In any case, the low-level fluctuations in the 0.4 GHz diffuse emission reported here raise the possibility that these might also be visible at substantially higher radio frequencies, even if not to 30 GHz. Evidence for such fluctuations in our companion DRAO 1.4 GHz observations is presently being analysed.

Such observational capabilities at both low and high radio frequencies should be possible with an appropriate version of the proposed SKA and the next generation of low frequency arrays. The possibility of distributed acceleration in the IGM also points to the need for a better understanding of plasma physics processes, such as large scale magnetic reconnection and similar field-to-particle energy conversion processes that might energize relativistic electrons over large regions of space. If some of the diffuse features in Figs. 2 - 5 are Galactic foregrounds as seems likely the consequently, much smaller, physical scales will permit

relativistic electrons to radiate locally at much higher frequencies for certain space-filling electron acceleration scenarios. In that case, some CMB foreground radiation at frequencies around  $\sim 30$  GHz is more likely.

The small scale features that we detect down to  $\sim 4'$  scales, and especially their polarized component (which we have not yet measured), are potentially important contributions to CMB foreground at high multipole scales ( $l$  of order  $\sim 1000$ ) at  $\sim 30$  GHz. The ultimate measurement of Stokes parameters I, Q, and U for any CMB foreground is important for isolating vector (B) modes in the CMB that are potentially important for tracing primordial, pre-recombination magnetic fields (e.g. Kosowsky & Loeb, 1996).

#### 4.7. Minimum temperature zones

Our images also show newly defined, “cold” areas at both  $2.8' \times 6.7'$ , and  $10' \times 10'$  resolution, which contain relatively few discrete radio sources. These are centered around ( $\alpha = 12^h 53^m$ ,  $\delta = +30^\circ$ , No. 1), ( $\alpha = 12^h 55^m$ ,  $\delta = +26.5^\circ$ , No. 2), and ( $\alpha = 13^h 05^m$ ,  $\delta = +28.5^\circ$ , No. 3). Each  $T_B$ -minimum zone is  $\sim 1^\circ$  or more in size. For regions (1), (2) and (3), the mean sky temperature levels are  $\sim 200$ ,  $+50$ , and  $-200$  mK respectively, after subtraction of the  $22\text{K} - 16\text{K}$  linear plane of “baseline” emission over our  $8^\circ$  field that was independently derived from the Haslam et al. all sky survey (Sec. 4.3). These residual “floor” temperatures are now comparable to each other even though they differ by  $2 - 4^\circ$  in location. This provides additional confirmation that these regions contain true extragalactic base temperature levels. As we show below, these minimum sky temperature levels also agree with predicted confusion levels from discrete extragalactic source counts at 0.4 GHz.

At the resolution of  $10' \times 10'$  (Figs. 4 and 5), the rms fluctuations in these colder zones,  $\sigma_{cold}$ , are about 0.2 K, less than 1 % of the broad Galactic emission that we have subtracted. We stress here that small “negative” temperatures in these zones do not represent a negative instrumental brightness, rather they are consistent with noise, and expected, being only of order  $\sigma_{cold}$  below the baseline level of  $T_B$ .

We now compare the rms  $\Delta T$  levels in zones (1) - (3) with the predictions of extragalactic point source confusion at 0.4 GHz. The rms confusion level at a frequency  $f_{GHz}$  for a FWHM of  $\theta'_1 \times \theta'_2$  can be approximated to,

$$\sigma_{conf} \simeq 0.17 \text{mJy} \times \theta'_1 \times \theta'_2 \times f_{GHz}^{-0.7} \quad (3)$$

(Condon, 1987). For a  $10' \times 10'$  beam and our average frequency of 0.42 GHz, equation (3) translates to  $\sigma_{conf} = 0.6$  K. After allowing for the subtraction of all recognizable point sources from the full resolution image of Fig. 2 before smoothing to the  $10' \times 10'$  resolution of Figs. 4 and 5, an rms confusion on the resultant image of  $\sim 0.25$  K is expected. This is close to the values measured.

## 5. SUMMARY AND CONCLUSIONS

We have described the first attempt to image a large field with a combination of the Arecibo radio telescope and the DRAO Interferometer, which have significant aperture overlap between the large single reflector and the interferometer. At resolutions as fine as  $3'$ , we can trace faint radio glow all the way to degree scales in the region of the North Galactic Pole. The radio glow to the west of the Coma cluster, region A, is likely to be, as we assume, at the distance of the Great Wall, in which case it traces CR electrons and magnetic fields out to the largest distance yet seen from a galaxy cluster. Limits to the synchrotron and IC radiative lifetimes at 0.4 GHz combined with the dimensions of region A suggest that the CR electrons are being accelerated, or re-accelerated, in intergalactic space. Such evidence from region A parallels that from the comparably sized lobes of individual giant radio galaxies (e.g. Kronberg et al. 2004). We have discovered a second, mostly diffuse feature (B) which, even though relatively bright in our images, has not been previously detected.

The origin of other degree-scale features is uncertain or unknown. They could be either faint, small scale, previously unmapped Galactic foreground features at the distance of the Great Wall, at greater intergalactic distances including blends of fainter discrete sources or, most likely, some combination of these. It appears that at least part of region A is at the distance of the Coma supercluster, implying that such glow regions should exist elsewhere in intergalactic space. A possible relationship to the “WHIM” awaits better specification of hot thermal gas in the IGM, e.g. via future EUV and X-ray images and high excitation X-ray line location.

A preliminary intercomparison of the radio features with both radio-loud and radio-quiet galaxies suggests that the diffuse radio glow is probing LSS in a different way to that defined by the large scale optical surveys of galaxies.

Intergalactic synchrotron emission presents an interesting opportunity to probe plasma conditions in the IGM, and especially intergalactic CR diffusion speeds. Our results suggest that reconnection, or some similar CR acceleration mechanism, is occurring to re-accelerate CR electrons in intergalactic space, as appears to happen within comparably sized giant radio galaxy lobes.

#### ACKNOWLEDGMENTS

We thank John Huchra for his assistance with the CfA catalog data, and Raul Cunha at the University of Toronto for his help with the figures. We acknowledge helpful discussions with T. Landecker, R.S. Roger, C.R. Purton, M. Wolleben, and A.G. Willis. This research was supported by the Natural Sciences and Engineering Research Council of Canada (PPK, RK), the U.S. Department of Energy through the LDRD program at LANL (PPK), and the National Research Council of Canada. The Dominion Radio Astrophysical Observatory is a National Facility operated by the National Research Council of Canada. The Arecibo Observatory is part of the National Astronomy and Ionosphere Center, which is operated by Cornell University under a cooperative agreement with the National Science Foundation.

## REFERENCES

- Briel, U., Henry, J.P., & Böhringer, H. 1992, *A&A*, 259, L31  
 Chokshi, A., & Turner, E. L. 1992, *MNRAS*, 259, 421  
 Colgate, S.A., & Li, H. 2004, *Comptes Rendus*, 5, 431  
 Colless, M., & Dunn, A.M. 1996, *ApJ*, 458, 435  
 Condon, J.J. 1987, *Proceedings of the Arecibo Upgrading Workshop*, Eds. J.H. Taylor, M.M. Davis, Cornell University, Ithaca, NY.  
 Condon, J.J., Cotton, W.D., Greisen, E.W., Yin, Q. F., Perley, R.A., Taylor, G.B., & Broderick, J.J. 1998, *AJ*, 115, 1693  
 Deiss, B.M., Reich, W., Lesch, H., & Wielebinski, R. 1997, *A&A*, 321, 55  
 de Lapparent, V., Geller, M. J. & Huchra, J. P. 1991, *ApJ*, 369, 273  
 Dolag, K., Grasso, D., Springer, V., & Tkachev, I. 2004, *J. Korean Ast. Soc.* 37, 427  
 Enßlin, T.A., Kronberg, P.P., Perley, R.A., & Kassim, N.E. 1999, in *Diffuse Thermal and Relativistic Plasma in Galaxy Clusters*, *MPE Report No. 270*, eds. Böhringer, H., Feretti L., & Schuecker P.: 271, 21  
 Finoguenov, A., Briel, U., & Henry, J.P. 2003, *A&A*, 410, 777  
 Furlanetto, S.R., & Loeb, A. 2001, *ApJ*, 556, 619  
 Gopal-Krishna, & Wiita P. J. 2001, *ApJ*, 560, L115-L118  
 Haslam, C.G.T., Stoffel, H., Salter, C.J., Wilson, W.E., 1982, *A&AS*, 47, 1  
 Henning, P.A. 1989, *AJ*, 97, 1561  
 Henry, J.P. 2004, *J. Korean Ast. Soc.*, 37, 374  
 Huchra, J. P., Geller, M. J., de Lapparent, V., & Corwin, H.G. Jr. 1990 *ApJ Suppl.*, 72, 433  
 Huchra, J. P. et al., 2004 *The CfA Redshift Survey* <http://cfa-www.harvard.edu/~huchra/zcat>  
 Kim, K. T., Kronberg, P. P., Giovannini, G., & Venturi, T. 1989, *Nature* 341, 720  
 Kim, K.-T., 1994, *A&AS*, 105, 403  
 Kim, K-T., Kronberg, P.P., Dewdney, P.E., & Landecker, T.L.: 1994, *A&AS*, 105, 385  
 Kosowsky, A. & Loeb, A. 1996 *ApJ*, 469, 1  
 Kronberg, P.P., Dufton, Q.W., Li, H., & Colgate, S.A.: 2001, *ApJ*, 560, 178  
 Kronberg, P. P., Colgate, S. A., Li, H., & Dufton, Q.W.: 2004, *ApJL*, 604, L77  
 Landecker, T.L., Dewdney, P.E., Burgess, T.A., 2000, *A&AS*, 145, 509  
 Miniati, F., Ryu, D., Kang, H., et al. 2000, *ApJ*, 542, 608  
 Nicastro, F., Mathur, S., Elvis, M., Drake, J., Fang, T., Fruscione, A., Krongold, A., Marshall, H., Williams, R., & Zezas, A. 2005, *Nature* 433, 495-498  
 Roger, R.S., Bridle, A.H., & Costain, C.H. 1978, *AJ*, 78, 1030  
 Ryu, D.S., Kang, H., & Biermann, P.L.: 1998, *A&A*, 335, 19  
 Sieber, W., Haslam, C. G. T., & Salter, C. J. 1979, *A&A Suppl.*, 74, 361  
 Sigl, G., Miniati, F., & Enßlin, T. A. 2004, *Phys Rev. D*, 70, 2004  
 White, S.D.M., Briel, U.G., & Henry, J.P. 1993, *MNRAS*, 261, L8  
 Willis, A.G., 1999, *A&AS*, 136, 603  
 Xu, Y., Kronberg, P. P., Habib, S., & Dufton, Q. W.: 2006, *ApJ* 637, 19

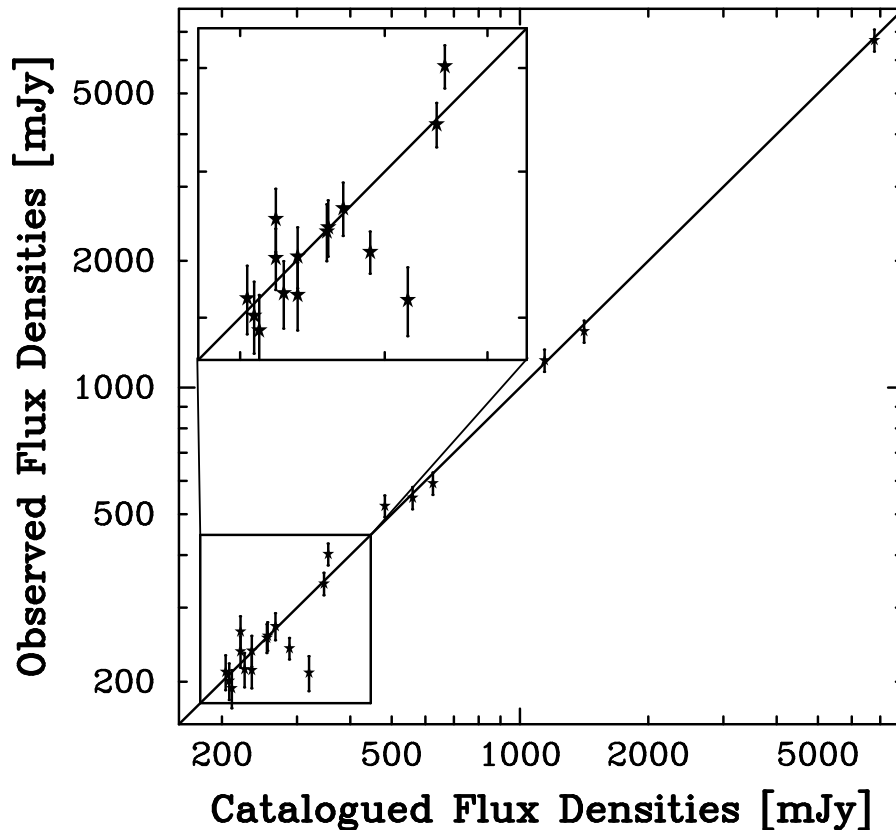


FIG. 1.— A comparison of flux densities for compact sources brighter than 200 mJy at 408 MHz between the present observations and the values published by Kim (1994).



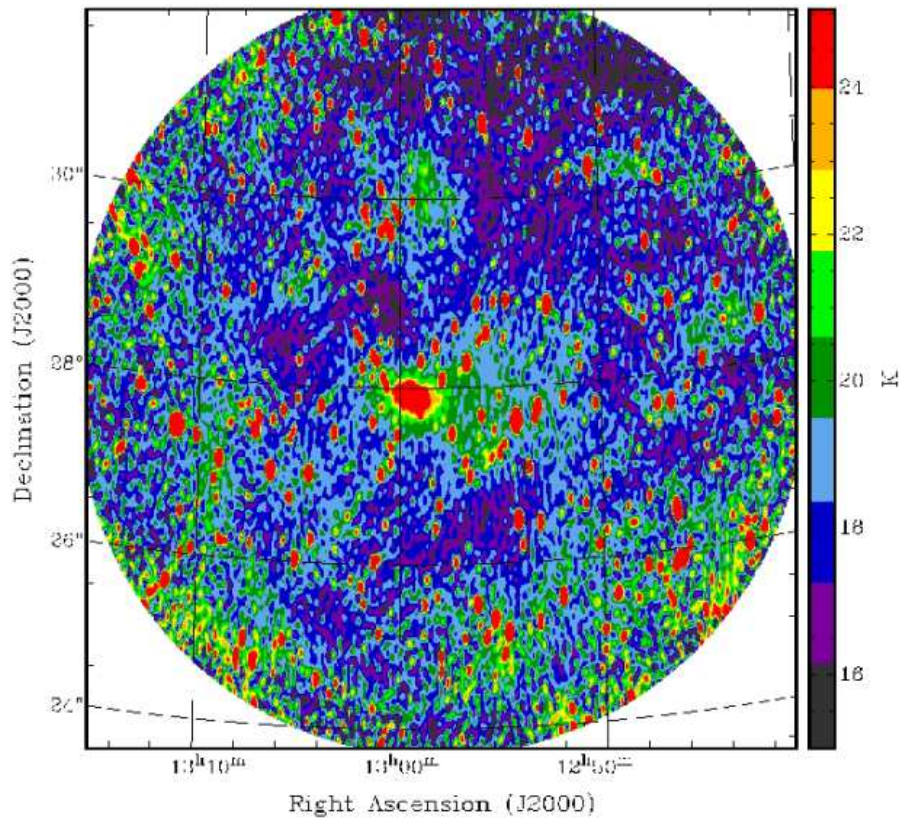


FIG. 2.— Radio continuum image at 408 MHz of an  $8^\circ$  diameter field within the Great Wall “filament” of galaxies centered near the Coma cluster. The half-power beamwidth is  $2.8' \times 6.7'$ , elongated N-S. The image contains discrete radio sources which are distinguishable at this resolution from patches of diffuse radio glow.

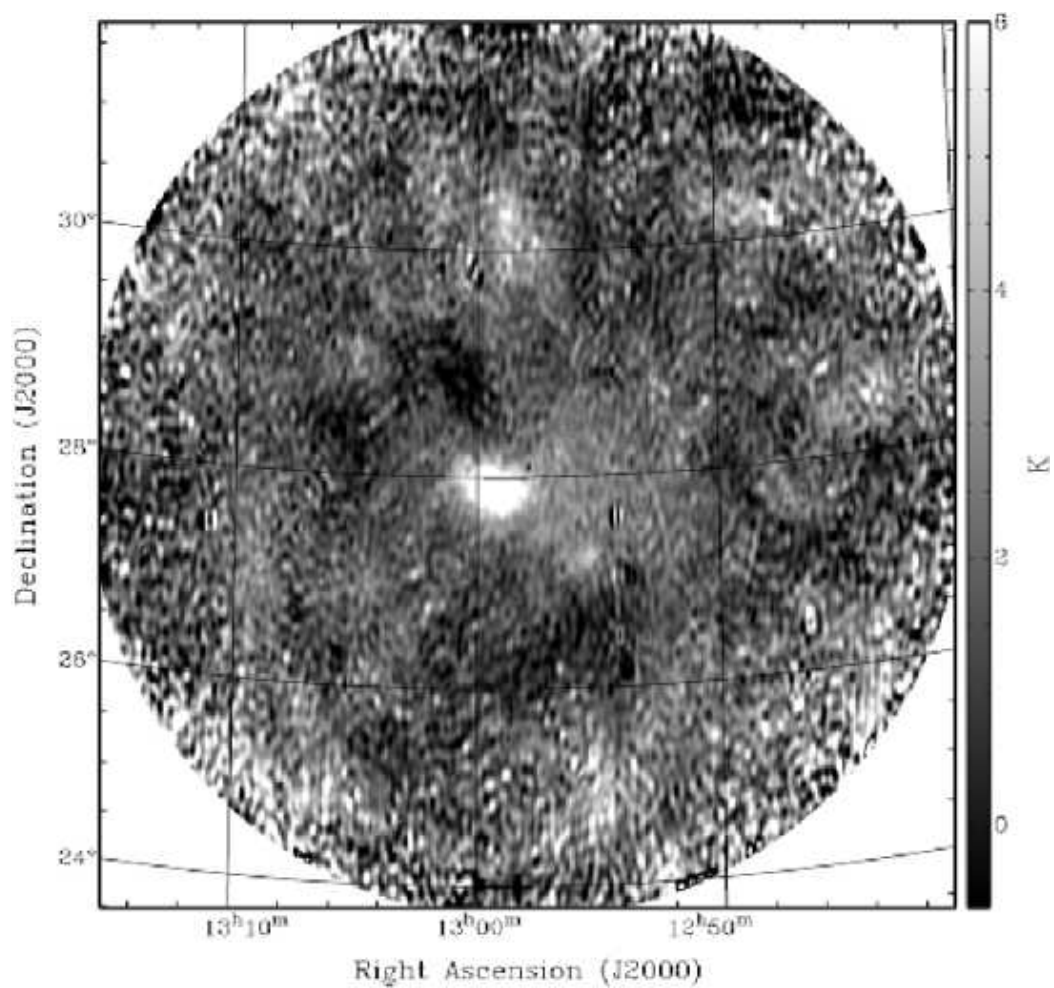


FIG. 3.— The same image and resolution as in Fig. 2, but with the discrete sources and a smooth (CMB + Galactic) background subtracted.

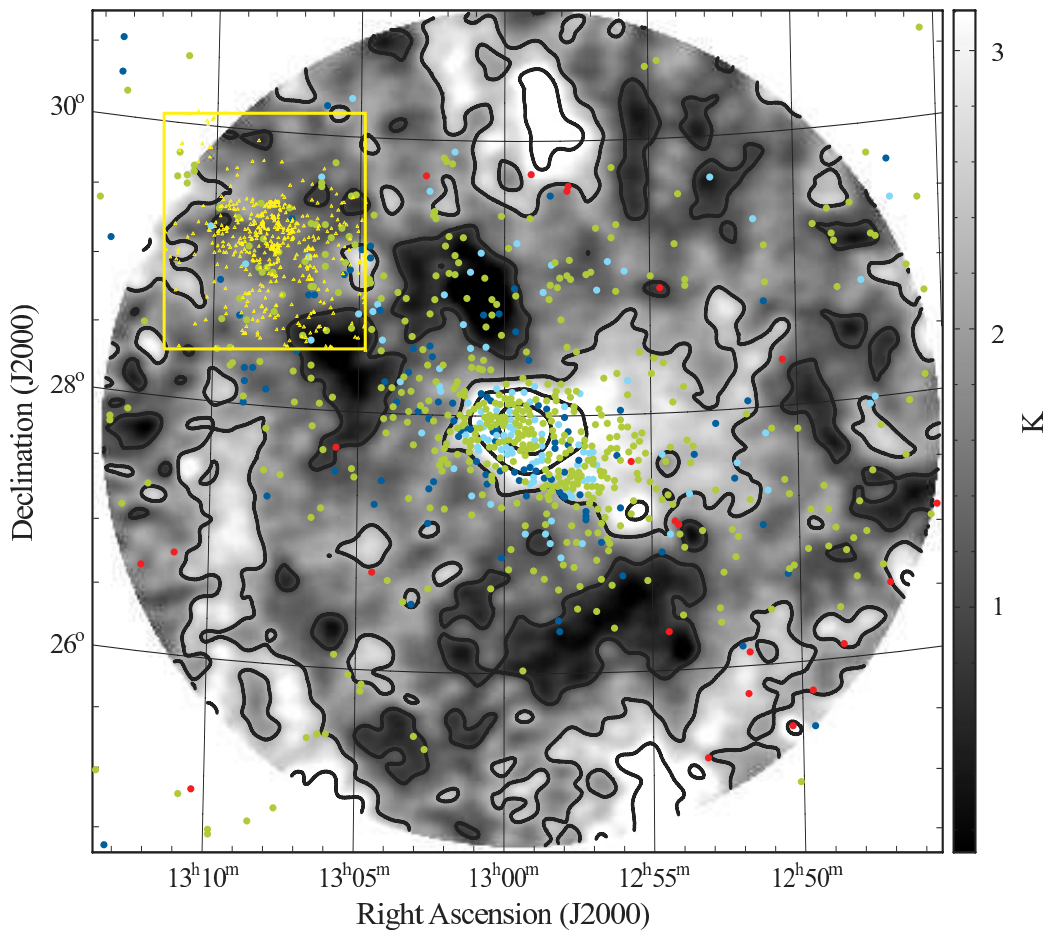


FIG. 4.— The radio continuum image of Fig. 3 in grey scale, convolved to a circular beam of half power width  $10'$ . Contours levels are at 1.0, 2.25, 3.5, and 10 K above the mean level of the three (comparable) coldest zones after subtraction of the distributed extragalactic component, the CMB, and a linear plane Galactic foreground. “Negative” values below this mean are only of order  $\sigma$  about this mean (see text). Overlaid are the positions of Coma supercluster galaxies from the CfA catalog from Huchra et al. (2004). The galaxy redshift coding is red for velocities below 4000 km/s, blue between 4000 and 6000 km/s, green between 6000 and 8000 km/s, and light blue between 8000 and 10,000 km/s. The yellow-coded points in the upper left inset box have radial velocities from 30,000 to 100,000 km/s, beyond the Great Wall, and are part of a CfA catalog extension (Huchra et al. 2004). The majority are a superposition of two concentrations around radial velocities of 38,000, and 70,000 km/s (see text).

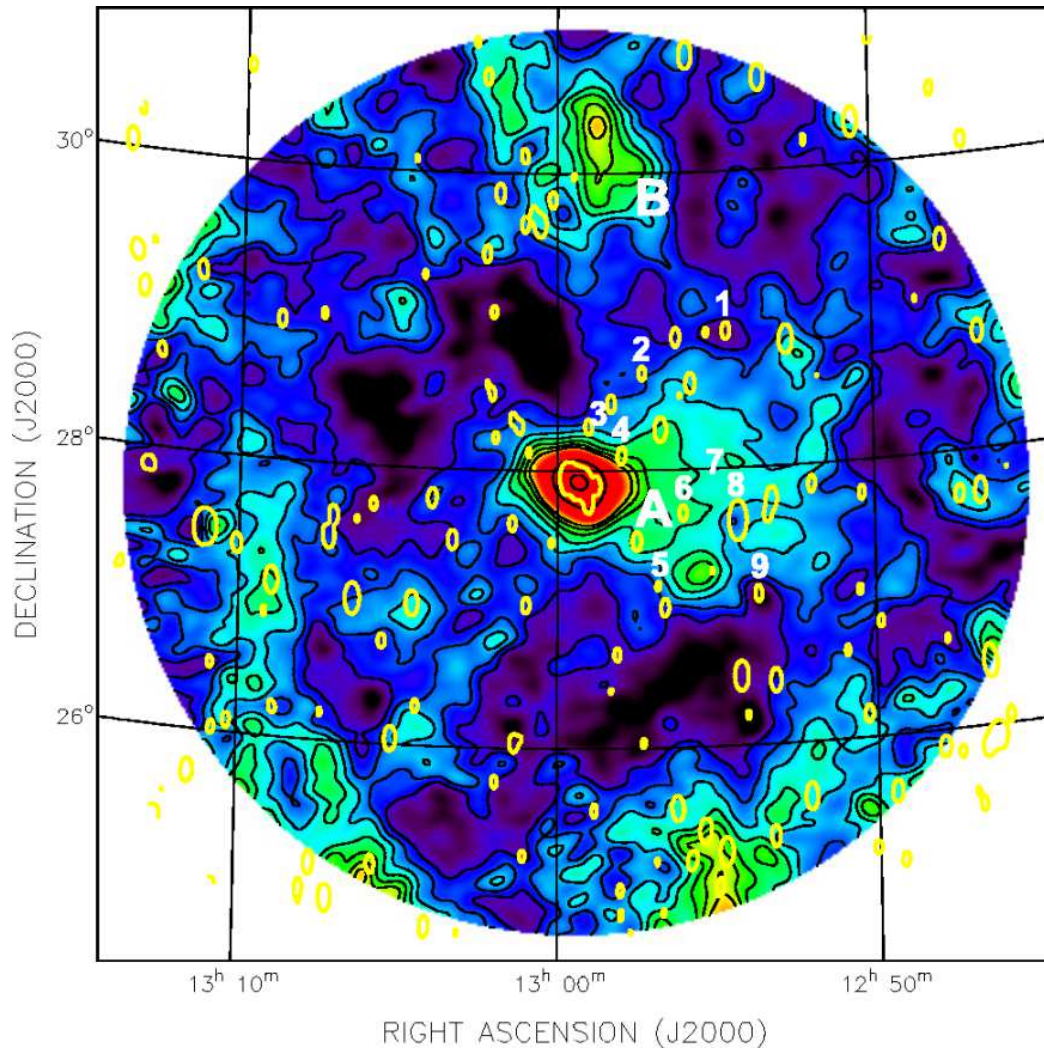


FIG. 5.— The radio continuum image convolved to  $10'$  as in Fig. 4, now showing the  $T_B$  levels in more detail, and overlaid with the brightest compact structures from Fig. 2. The black contours are shown at 1.4, 1.9, 2.4, 2.9, 3.4, 3.9, 4.4, 10, 40 K above the same reference level as for Fig. 4. Yellow contours are overlaid to indicate the brighter discrete sources in the original map of Fig. 2. The numbered radio galaxies and their radial velocities are selected from Table 8 of Kim et al. (1994). They are (name, radial velocity in  $\text{km s}^{-1}$ ): 1. N4793, 2465; 2. Zw160-58, 7649; 3. N4848, 7248; 4. anonE/S0, 8160; 5. N4827, 7356; 6. Zw160-20, 4900; 7. Zw160-15, 7470; 8. 3C277.3, 25583; 9. N4789, 8300. (Refer to discussion in text.)